Transactions on Energy Systems and Engineering Applications

Article

Harmonic mitigation of PV-based resonant Cuk converter using lightning search optimization

M. Ulaganathan[1,*], R. Muniraj[1], Natarajan Karuppiah[2] and Patil Mounica[2]

[1] Department of Electrical and Electronics Engineering, P.S.R. Engineering College, Sivakasi, India.
[2] Department of Electrical and Electronics Engineering, Vardhaman College of Engineering, Shamshabad, Hyderabad, India.
[*] Correspondence: ulagu.er@gmail.com

Received: 04 July 2024; Accepted: 07 April 2026; Published: 02 June 2026

Abstract: In today's situation, renewable power is an important one, mainly owing to the shortage of fossil fuels. One of the future's non-conventional energy sources is solar power. But the changing weather condition introduces problems of power quality like harmonic fluctuation, voltage dip, reliability troubles and deviations in voltage waveform, which affect the stability of the entire grid. In this work, the PV (photovoltaic) panel is linked with the grid via a ZVT (Zero Voltage Transition) - ZCT (Zero Current Transition) CUK Converter and a 3-level 3ϕ Voltage Source Inverter (VSI). Here the converter's conduction loss and switching loss were eliminated using the ZVT–ZCT principle. Here the resonant components are placed in diagonal as switches. This one to one placement will reduce the conduction loss and switching loss in the converter. Converter switching is done by using MPPT (Maximum Power Point Tracking) - based Incremental Conductance-Integral Regulator algorithm and the Inverter Switching is done by using PI tuned Optimization. This work proposes Lightning Search Optimization (LSA) with VSI (Voltage Source Inverter) to solve harmonic problems in the Renewable energy system. MATLAB / Simulink is used to simulate the proposed system. This proposed Optimization technique is employed to lessen the THD by 0.349% and increase the system efficiency to 99.35%. The Quasi Resonant Cascade converter is compared with the Resonant LUO, BOOST and SEPIC converters.

1. Introduction

There are two types of energy sources available such as non-renewable and renewable energy sources. Due to its widespread availability and suitable application in producing power, solar energy is particularly well-liked. A converter of resonant SEPIC was used to regulate the output voltage with good efficiency [1]. A PV system is linked to the grid using a three-phase inverter and a two-phase closed-loop control system. External DC power control is used to work with the internal control circuit's output current and voltage,

How to cite this article: Ulaganathan, M.; Muniraj, R.; Karuppiah, Natarajan; Mounica, Patil. Harmonic mitigation of PV-based resonant Cuk converter using lightning search optimization. *Transactions on Energy Systems and Engineering Applications*, 7(1): 707, 2026. DOI:10.32397/tesea.vol7.n1.707

which ensures the power status of the system [2]. In addition, due to smooth transmission techniques, size and cost are reduced, compared to traditional boost converters.

LCL Resonant tank shows the ability of DC voltage conversion, effectively controlling the specified value. It appears to provide zero voltage and zero current on the phase control converter; however, the quench current is high. A semi-resonant single-converter is recommended for high performance [3]. This converter operates in the desired transmission mode to smoothly switch the power semiconductor switches using variable switching frequency control [4].

Various types of adjustable voltage converters are considered. To confirm the effectiveness and to evaluate the suggested converter type, a mathematical description of the building of buck converters with zero current switching is proposed for high voltage applications [5]. This study introduces a resonant CUK converter that functions across a large input and output voltage range and at exceptionally high frequencies. For the power cycle battery pack, the CUK converter proposes a charging solution based on a Fed-resonant LLC converter, where the CC/CV (constant current /constant voltage) charging algorithm is implemented by LLC converter inverter logic [6]. To ensure the dependability of these translators, critical parameters are initially acquired to estimate the reliability factors. Most of them use the vertical conversion technique to achieve their goals, especially in modern multi-generation converters. Switch topologies are easy to control, but it is widely recognized that power losses outweigh switching topologies [7].

The investigated linear PI (proportional-integral) controller was designed and applied to control a semi-resonant buck converter of 54 V, 2.916 kW. The PI controller algorithm consists mainly of two parameters, relative gain (Kp) and integral time (Ki), to provide adequate control performance tuned to the form [8]. MPPT is a useful method for harvesting PV energy at different locations. However, balancing tracking speed and swing requirements with typical P&O and constant turbulence is difficult [9]. Adaptation of P&O strategies are proposed as a solution to these problems. None of these allows variable-frequency tuning for resonant transformers [10]. The article presents a reconstruction of the MPPT midpoint with dynamic frequency perturbations. The proposed system solves common P&O problems using simple mathematics. To solve the nonlinear complex problem LSA is selected to use [11].

The work proposes Lightning Search Optimization (LSA) with VSI to solve harmonic problems in the Renewable energy system. Here the proposed work's block diagram is discussed in Section 2. Section 3 explains the optimization technique. Section 4 displays the Simulation results and finally, section 5 shows the conclusion.

2. Description of the Proposed work

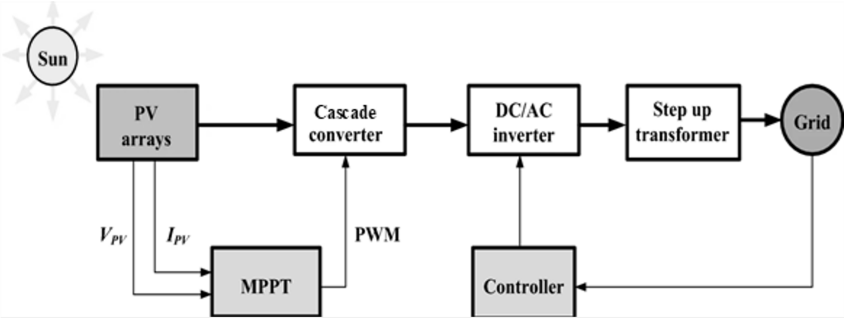

Figure 1. Block diagram of the proposed system.

The RES system used is photovoltaic. The PQ problems are created by sudden loads or unplanned loads in the system. For this reason, the mismatches of the reactive power and weakening of the voltage were

created. Thus this proposed paper solve the sag of the voltage and sag of the current and also the THD. Voltage Source Inverter (VSI) is a component of the RES system that addresses these issues [12]. The LSA optimization is used. Figure 1 presents the block diagram representation of a resonant Cuk converter, which comprises of a controller and a PV-linked quasi-resonant cascade converter that is linked to the grid via an inverter.

From the PV, the Optimized Supervised MPPT Controller regulates the maximum current and voltage. In rapidly changing weather conditions, the INC-based MPPT method gives the best performance and excess power generation as the INC-IR is incorporated into the photovoltaic system branch.

Using these quasi resonant converters, the losses of switching are reduced. This keeps transient response small and improves system efficiency and performance. The switching technology is applied to switches of the semi-resonant converter. ZVT (zero voltage transmission) and ZCT (zero current transmission) are the switching technologies. Due to this ZCT-ZVT conversion, resonant components with lower values are used. Here diagonally the resonant components are placed in the switches. This placement will reduce the losses of conduction and switching in the converter. The proposed work is related to VSI. Here, the control of inverter switches is implemented using techniques that increase accuracy and integration. System performance and harmonics are reduced by using the LSA. The output of the inverter is AC. This is used in the grid. The voltage signal is controlled by a PI controller before being passed to a PWM generator, which produces a PWM signal for the power supply system.

2.1. Photovoltaic System

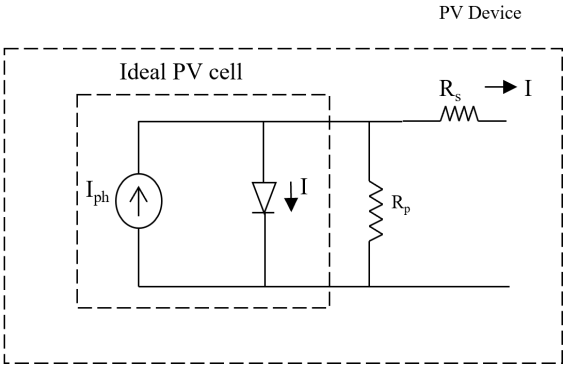

Figure 2. Circuit diagram of PV.

The circuit model of the PV electrical model is shown in Figure 2. Here the circuit diagram consists of a Photo electric current I_{ph}, and the parallel resistance R_p, R_s is the series resistance and I is the Diode current.

The PV cell V-I characteristics-based Equation is as follows,

$$I = I_{ph} - I_s \left[\exp\left(\frac{q(V + R_{se}L)}{kT_cA} \right) - 1 \right] - \frac{V + IR_s}{R_{sh}}. \tag{1}$$

Here I_{ph} is the photoelectric current. The corresponding model is reported in the below formula

$$I = N_P I_{ph} - N_P I_s \left[\exp\left(\frac{qV}{N_S k T_C A} \right) - 1 \right], \tag{2}$$

where the series connected is N_s and N_p is the parallel connected of the PV array.

2.2. CUK Converter topology

The proposed CUK-based DC-DC converter topology uses C_L coupling capacitors in Critical Conduction Mode (CRM), which allows the designer to use dense film capacitors instead of bulky and unstable electrolytic capacitors and consequently extend the service life of the switch [13].

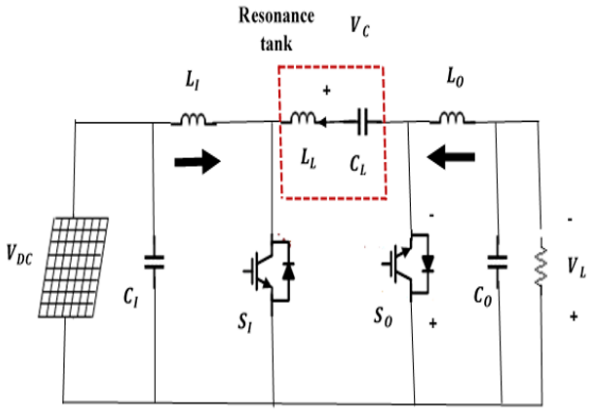

Figure 3. Proposed auxiliary CUK converter.

To prevent the voltage across S0 from falling at t2, the contact voltage must be suppressed and V_C limited at this time. This is done by connecting the diode and finding a suitable slot. Figure 3 shows the proposed auxiliary Cuk converter. Steady-state waveforms of ZCT CUK converter is presented in Figure 4.

Interval 1: (t0-t1)

During this time, S1 is turned off, and the input current in each switching circuit cuts through the nominal DC contact capacitance C_L.

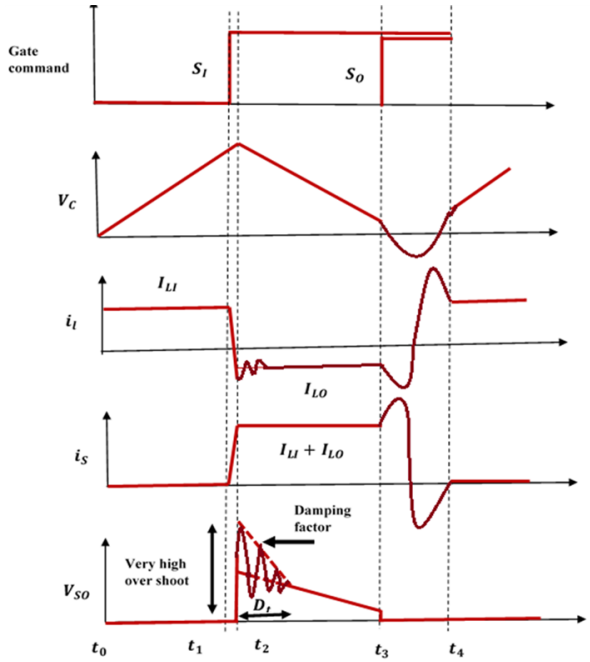

Figure 4. Steady-state waveforms of ZCT CUK converter.

Interval 2: (t1-t2)

The connecting elements, which are the series connection between C_L and L_A, short circuit and start bouncing when S1 is turned on. Both the state-level diagram and the equivalent diagram of the converter used in this technique are displayed in Figure 3. At the same time, the current through parallel diode S2 (D2) gradually becomes zero. This is the point where $I_L - I_o$ splits. Since S2 is missing from the ZCS, the effects of inverse recovery are neglected [14].

The voltage of the link inductor and the link capacitor can be defined at this time.

$$I_{LA}(t) = I_I \cos\left(\frac{t-t_1}{\sqrt{L_A C_L}}\right) - \frac{V_C(t_1)}{\sqrt{\frac{L_A}{C_L}}} \sin\left(\frac{t-t_1}{\sqrt{L_A C_L}}\right), \tag{3}$$

$$V_C(t) = V_C(t_1) \cos\left(\frac{t-t_1}{\sqrt{L_A C_L}}\right) - I_I * \sqrt{\frac{L_A}{C_L}} \sin\left(\frac{t-t_1}{\sqrt{L_A C_L}}\right), \tag{4}$$

where,

$I_{LA} \rightarrow$ the current of the auxiliary inductor.

$I_I \rightarrow$ decreasing from its initial value.

Interval 3: (t2-t3)

When D2 is in off condition, the resonance cycle changes dramatically. In resonant small-signal mode, it closes the path through the input switch, so it has no effect on the audio circuit and can be left out. The voltage across I_L and C_S present across the auxiliary coil is shown in the state parameters in the state-level diagram.

The state parameters start to resonate from their initial values, which, in this resonance interval, are identical.

$$I_L(t_2) = -I_O, \tag{5}$$

$$V_C(t_2) = 0, \tag{6}$$

where,

$C_S \rightarrow$ the placed in series.

$C_L \rightarrow$ the placed the capacitance value.

Resonant tank elements are illustrated with current and voltage;

$$I_L(t) = -I_O - \frac{V_C(t_2)}{\sqrt{\frac{L_A}{C_S}}} \sin\left(\frac{t-t_2}{\sqrt{L_A C_S}}\right), \tag{7}$$

$$V_{C_S}(t) = V_C(t_2) - V_C(t_2) \cos\left(\frac{t-t_2}{\sqrt{L_A C_S}}\right), \tag{8}$$

where,

$V_C(t_2) \rightarrow$ the voltage of the link capacitor.

Interval 4: (t3-t4)

This is the power transfer mode where the stored power of C_L is applied to the output load. During each switching cycle, the output current, which is assumed to be constant, flows into and out of the junction; due

to this, the capacitor voltage decreases. At the beginning of this interval, the auxiliary switch SA and diode DA are equal.

$$I_S = I_{LA-max} - I_{out}. \tag{9}$$

2.3. Pulse Control of VSI Using Optimization Technique

Figure 5 shows the VSI schematic representation. Six Switches composed the VSI. The Switches are $S_{inv,1}$ to $S_{inv,6}$. The inverter of each leg middle is connected to each phase. The six switches are controlled by using the proper PWM switching. In this work, the switching is done by the PI Controller. To avoid the DC short circuit each leg switches are connected interchangeably.

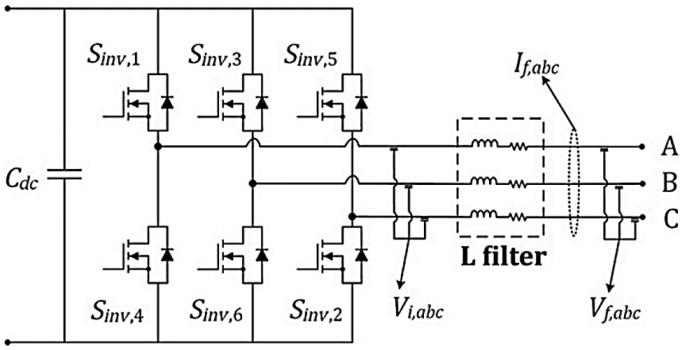

Figure 5. Voltage source inverter schematic representation.

The VSI output side dynamic equation is

$$V_{i,abc} = V_{f,abc} + L_f \frac{d_{f,abc}}{dt} + R_f I_{f,abc} \tag{10}$$

where R_f is per phase resistance, L_f is per phase Inductance, $V_{f,abc}$ is the output voltage of 3ϕ inverter, $I_{f,abc}$ is the output current of 3ϕ inverter, and $V_{f,abc}$ is the filter output voltage.

The working of the Harris Hawks optimization techniques is below,

Step 1: Initialization

Initialize the K_p and K_i, which are the PI controller gain parameters, the voltage command of the inverter, duty cycle and the population size are initialized as $V_{in}(t)$ and D.

Step 2: Random Generation

The gain is chosen at random and it is in the following equation,

$$x_i = \begin{bmatrix} K_p^1 K_i^1 & K_p^2 K_i^2 & \cdots & K_p^n K_i^n \end{bmatrix} \tag{11}$$

Step 3: Evaluation of Fitness Function

It is applied to each particle and the fitness value was evaluated with the initial random population. Integral Square Error (ISE) is determined by the given Equation.

$$ISE = \int_0^T e^2(t)\, dt \tag{12}$$

Step 4: Position Updating

Using the fitness function basis, the Hawks' position is updated,

$$X_I^j = X_{Min}^j + rand\,[0,1]\left(x_{Max}^j - x_{Min}^j\right), \tag{13}$$

here, x_{ij} is displayed as the solution of the neighborhood.

Step 5: Iteration

The limit of iteration is tested, if the iteration range is maximum then stop, else go back to step 2.

Step 6: Termination

At the end of the HHO procedure minimize the fitness function.

3. Optimization Technique

The Proposed MPPT technique is Incremental conductance obtained using the integral regulating technique to optimize the maximum power point. The Quasi Resonant Converter is linked to the three-phase VSI. Here, LSA is employed to increase system efficiency and to decrease harmonics. The challenge with optimization is trying to identify the ideal solution.

3.1. LSA (Lightning Search Algorithm)

This algorithm is used to solve the nonlinear complex problems. This is based on the algorithms of metamorphic. It has searching behavior. It finds the shortest path between the initial point and the final point. Here explained the three projectiles. They are transition, space and lead [15, 16].

Transition Projectile: The first part of the establishment of the performance leaders is the introduction of the unplanned entries of the change. It can be set as a random number using equally distributed space.

$$f(x^T) = \begin{cases} \dfrac{1}{b-a} & for\ a \le x^T \le b \\ 0 & elsewhere \end{cases}, \tag{14}$$

where x^T is the step leader energy of the initial tip. SL is an abbreviation of the Step leader. Where the initial tip energy of the step leader is denoted as x^T. The step leaders are denoted as SL, for a population N, is given as $sl_1, sl_2, sl_3, \ldots, sl_N$, N random projectiles $[P^T = P^{T_1}, P^{T_2}, P^{T_3}, \ldots, P^{T_N}]$.

Space Projectile: In this leading leader is used to find. Space projectile p^S position = $[P^{S_1}, P^{S_2}, P^{S_3}, \ldots, P^{S_N}]$

$$f(x^s) = \begin{cases} \dfrac{1}{\mu} e^{\left(\frac{-x^s}{\mu}\right)} & for\ x^s \ge 0 \\ 0 & for\ x^s \le 0 \end{cases}. \tag{15}$$

Therefore, the $[P^{S_i}$ at step $+1$ is represented by: $p_{i-New}^s = p_i^s \pm exprand(\mu_i)$

Lead Projectile: This projectile motion is close to the ground.

$$f(x^L) = \frac{1}{\sigma\sqrt{2\pi}} e^{\frac{(-x^L-\mu)^2}{2\sigma^2}}. \tag{16}$$

3.2. HRES using LSA

It is used to minimize the objective function. The objective function is denoted as below,

$$Minimize\ F = \sqrt{\frac{\sum_{k=1}^{N}\left[p_k^{observed} - p_k^{forecasted}\right]^2}{\sum_{k=1}^{N}\left[p_k^{observed}\right]^2}} * 100\% \tag{17}$$

where the number of articles used is denoted as N, $p_k^{observed}$ is defined as observed power at Kth iteration, and $p_k^{forecasted}$ is defined as the predicted power at Kth iteration.

4. Simulation Results

This section reports the observations from the simulation and discusses the voltage control in the sources of energy that are renewable using the proposed techniques. Using MATLAB Simulink, the suggested system is realized. The proposed strategies and the effectiveness of existing strategies are analyzed. The Simulink representation of the HRES system is shown in Figure 6. The VSI is controlled by using Lightning Search Optimization techniques. To escalate the power quality of the device connected to the renewable system Voltage source inverter-based control technique is used. Figure 7 presents the modelling of the PV system. In this, The PV waveform voltage is 300 V and the produced current is 50A. PV Current and voltage waveform are shown in Figure 8.

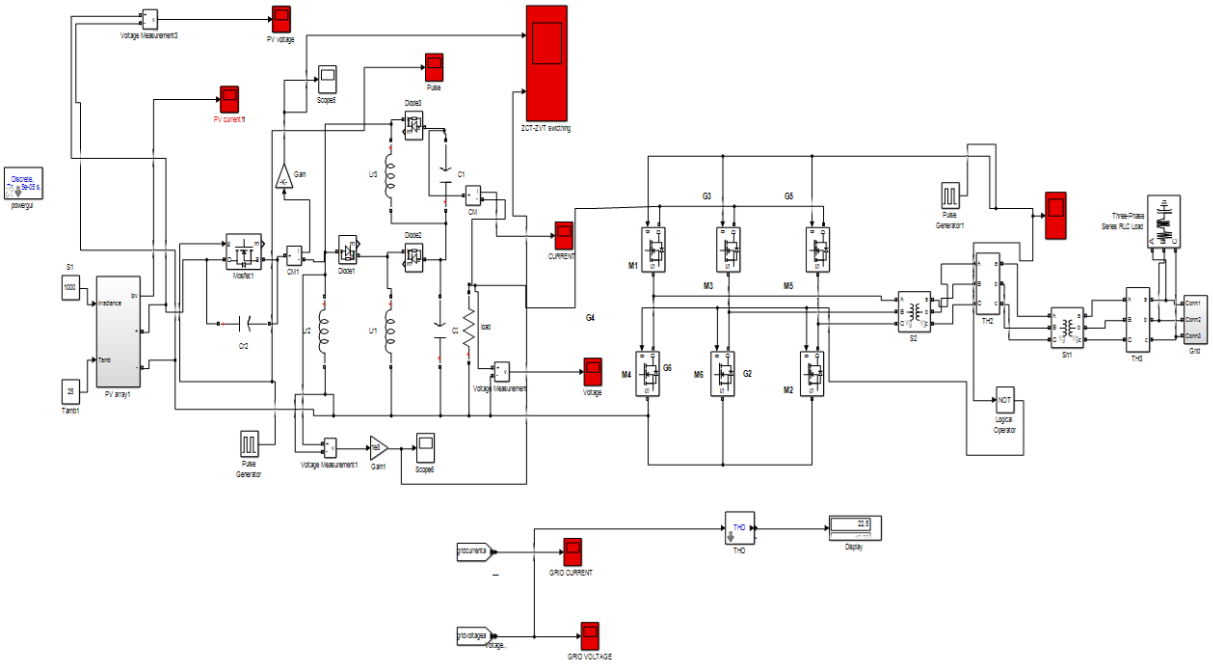

Figure 6. Simulink representation of the HRES.

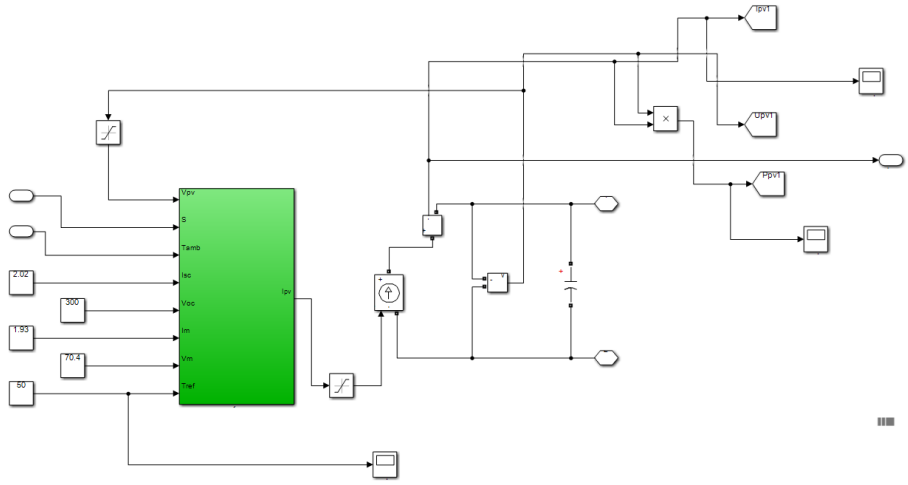

Figure 7. Subsystem modelling of PV system.

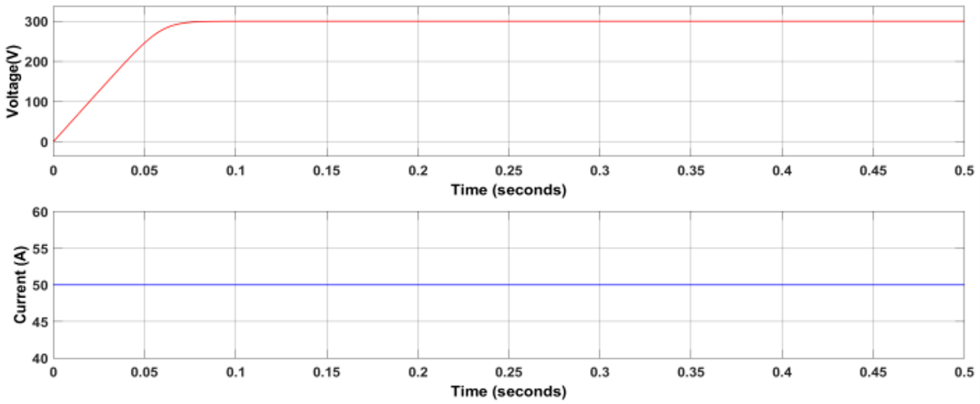

Figure 8. Voltage and current of PV.

Table 1 shows the various converter parameters and Table 2 shows the LSA algorithm selected parameters.

Table 1. Parameters of proposed converter.

Parameters	Values
Input voltage	300V
Resistor, R	100Ω
Inductor	210μH
Switch	MOSFET IRF830
Capacitor	1 μF

Table 2. Parameter value selected for algorithm.

LSA parameters	
Parameter	**Value of Parameter**
Iterations	500
Rabbits	30

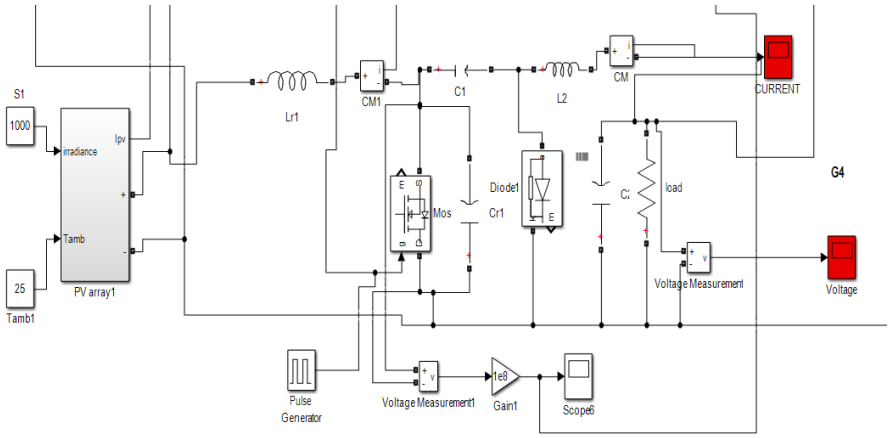

Figure 9. Simulink representation of the resonant Cuk converter.

In this Simulink consists of two inductors, switches, two capacitors and a diode. Here the resonant Cuk converter is getting input from the PV. PV provides DC output. The harmonic reduction happens in the VSI. VSI is used to control the LSA. LSA provides gain values. Gain values are taken and operated by the PI controller. The Cuk resonant converter Simulink representation is shown in Figure 9.

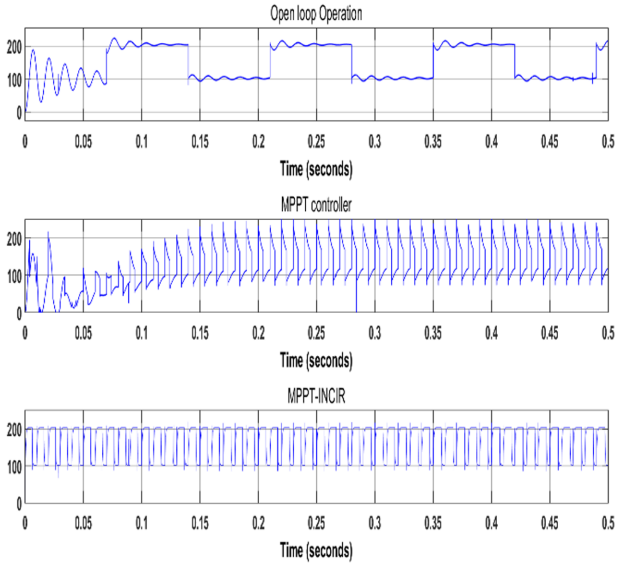

Figure 10. Soft switching of ZVT.

Converter Operation-The converter is a Cuk converter. Here the Cuk converter output is always greater than the input voltage. The proposed converter is linked with the resonant circuit to reduce the losses in the circuit. Using the proper converter switching operation the losses are reduced. The results are compared with the without MPPT and MPPT with basic Perturb and Observe. The Voltage switching and current switching is shown in Figure 10 and Figure 11, respectively. The obtained switching losses of the converter using various MPPTs are as follows. 4.3W is obtained without using MPPT algorithm, with MPPT algorithm the obtained switching loss is 2.78W. MPPT-INCIR provides 2.1W switching losses. The proposed MPPT-INCIR method reduces the switching losses.

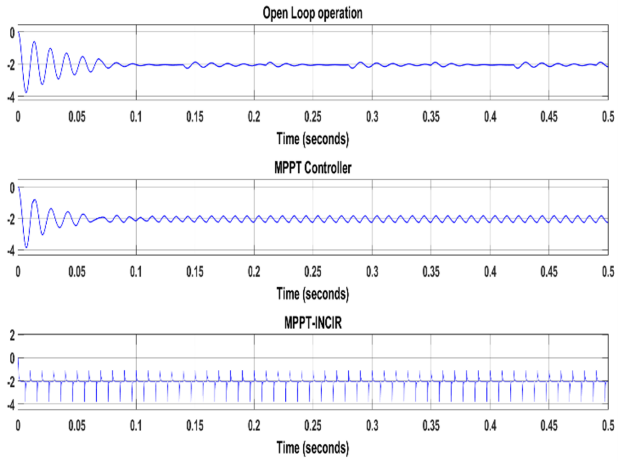

Figure 11. Soft switching of ZCT.

Here 450V for the obtained converter output voltage and the current is 76.7A. Figure 12 presents the Resonant Cuk voltage waveform. The current Waveform of Resonant Cuk is presented in Figure 13. The output voltage oscillates while the system is operating in a closed loop. So to reduce this oscillation go for the controller. Here MPPT controller is used to controlling the oscillations. Therefore, using the MPPT-INC-IR method produces the rise time, settling time and the Overshoot is low.

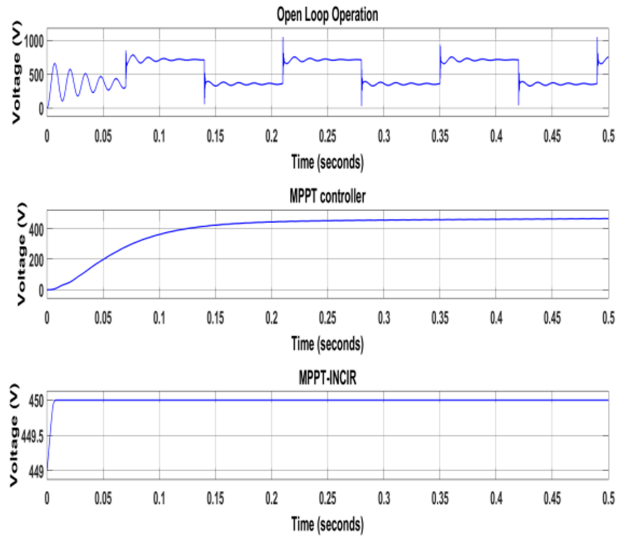

Figure 12. Output voltage of the resonant Cuk converter.

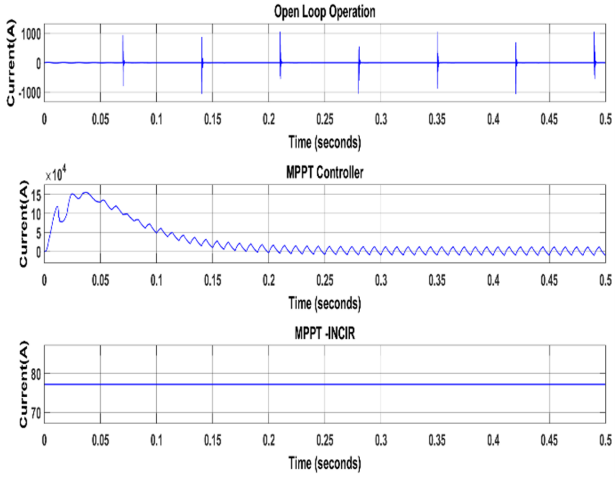

Figure 13. Output current of the resonant Cuk converter.

Grid voltage and current are compensated by using the PI. Here PI tuned LSA is proposed. It controls the VSI. So the harmonics are reduced, and 415 V transmission line voltage and 50Hz frequency are provided. Figure 14 and Figure 15 show the voltage and current of the grid respectively.

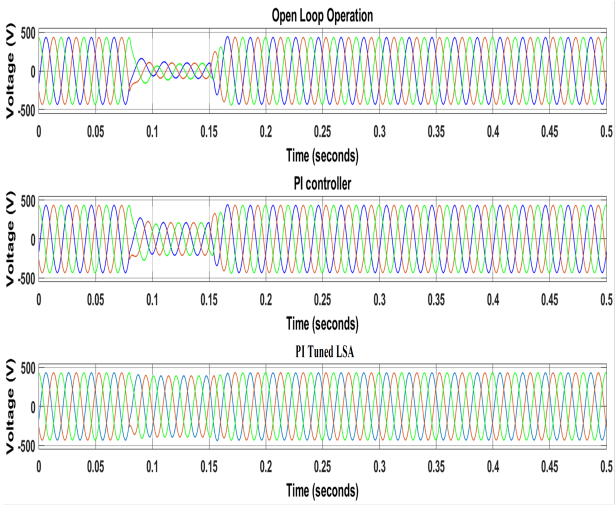

Figure 14. Grid voltage.

The Harmonics are observed from the grid waveform. For the periods 0.8sec to 0.15 sec, the voltage is under sag mode. It is rectified by using the PI-tuned LSA. Here handled three operations, are open loop, closed loop using PI Controller, and PI-tuned LSA. Here 12.56% THD is observed in Open loop operation. Closed loop using PI 2.45% is observed and finally, the proposed PI tune LSA produced 0.349% THD. It is very low compared to the other two.

Here using the ZCT-ZVT principle the losses (Switching and Conduction) are minimized. Here CUK converter has a MOSFET switch. The losses are measured across the switches. Its unit is W. The Calculation switching loss has the following equation.

$$P_{sw} = \frac{1}{2}\left(V_{IN}.I_O.[t_r + t_f].f_{sw}\right) \tag{18}$$

From the above equation 2.0MHz is the switching frequency values and it's denoted as f_{sw}, the MOSFET rise and fall time is denoted as t_r and t_f, respectively. Its value is 4nsec and 6nsec, respectively. The obtained switching losses are displayed in Table 3.

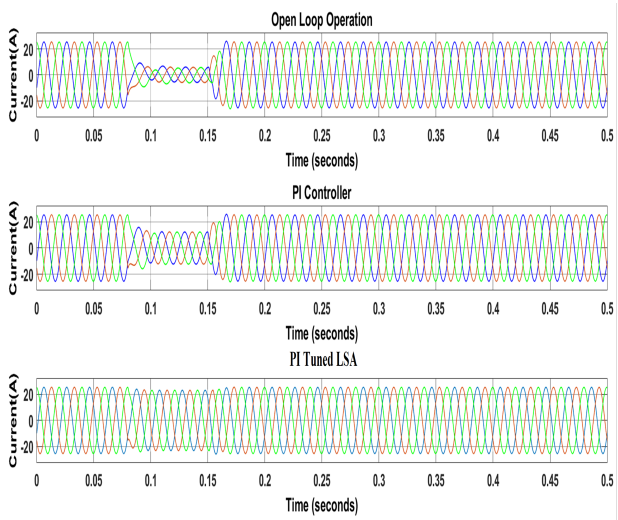

Figure 15. Grid current.

Table 3. Switching loss calculation.

Mode of Operation	CUK (W)
Open loop	4.3
MPPT –P&O	2.78
MPPT based INC-IR	2.1

Table 4. Performance specification of resonant converters.

Converters	Rise Time (Sec)	Settling Time (Sec)
LUO [3]	0.008	0.01
BOOST [7]	0.003	0.006
SEPIC [12]	0.003	0.005
Proposed	0.00001	0.0001

5. Conclusion

The proposed Quasi Resonant Cascade converter is compared to the existing Quasi Resonant LUO, BOOST and SEPIC Converter. The Switching of ZVT and ZCT is utilized to limit the switching losses. By reducing the switching losses, the system performance is improved. VSI control is employed with PI controller tuned Lightning Search Optimization technique. This proposed Optimization technique is employed to lessen the THD is 0.349% and Increase the system efficiency is 99.35%. The Quasi Resonant Cascade converter is compared to the Resonant LUO, BOOST and SEPIC converters. For this comparison, results show the proposed cascade converter has less settling time compared to the other LUO, BOOST and SEPIC converters.

Funding: This research received no external funding.

Author contributions: Conceptualization, M. Ulaganathan and R. Muniraj; Methodology, software, formal analysis, investigation, data curation, visualization, and writing—original draft preparation, M. Ulaganathan; Validation, writing—review & editing, Natarajan Karuppiah and Patil Mounica; Supervision, resources, and project administration, R. Muniraj.

Disclosure statement: The authors declare no conflict of interest.

Data Availability Statement: No data available to this article.

References

[1] Zhiliang Zhang et al. Analysis and decoupling design of a 30 MHz resonant SEPIC converter. *IEEE Transactions on Power Electronics*, 31(6):4536–4548, 2015.

[2] S. Jayaprakash et al. Comparison of solar based closed loop DC-DC converter using PID and ANN control for shunt motor drive. *International Journal of Power Electronics and Drive Systems*, 10(3):1324, 2019.

[3] Yuqi Wei, Quanming Luo, and Alan Mantooth. Overview of modulation strategies for LLC resonant converter. *IEEE Transactions on Power Electronics*, 35(10):10423–10443, 2020.

[4] Ngoc Dat Dao and Dong-Choon Lee. High-efficiency hybrid LLC resonant converter for on-board chargers of plug-in electric vehicles. *IEEE Transactions on Power Electronics*, 35(8):8324–8334, 2020.

[5] Jingying Hu et al. High-frequency resonant SEPIC converter with wide input and output voltage ranges. *IEEE Transactions on Power Electronics*, 27(1):189–200, 2012.

[6] Cheng-Yu Tang et al. An optimal frequency-modulated hybrid MPPT algorithm for the LLC resonant converter in PV power applications. *IEEE Transactions on Power Electronics*, 37(1):944–954, 2022.

[7] Junjun Deng et al. Frequency and parameter combined tuning method of LCC–LCC compensated resonant converter with wide coupling variation for EV wireless charger. *IEEE Journal of Emerging and Selected Topics in Power Electronics*, 10(1):956–968, 2022.

[8] J. R. Espinoza and G. Joos. Current-source converter online pattern generator switching frequency minimization. *IEEE Transactions on Industrial Electronics*, 44(2):198–206, 1997.

[9] Rahul Pandey and Bhim Singh. A power-factor-corrected LLC resonant converter for electric vehicle charger using Cuk converter. *IEEE Transactions on Industry Applications*, 55(6):6278–6286, 2019.

[10] Ashish Shrivastava and Bhim Singh. PFC Cuk converter based electronic ballast for an 18 W compact fluorescent lamp. In *2010 5th International Conference on Industrial and Information Systems*. IEEE, 2010.

[11] Shouxiang Li, Yifei Zheng, and Keyue Ma Smedley. A family of step-up resonant switched-capacitor converters with a continuously adjustable conversion ratio. *IEEE Transactions on Power Electronics*, 34(1):378–390, 2019.

[12] B. R. Lin and C. L. Huang. Zero voltage switching active clamp buck-boost stage Cuk converter. *IET Electric Power Applications*, 1(2):173–182, 2007.

[13] Laith Abualigah et al. Lightning search algorithm: a comprehensive survey. *Applied Intelligence*, 51:2353–2376, 2021.

[14] Daocheng Huang, Shu Ji, and Fred C. Lee. LLC resonant converter with matrix transformer. *IEEE Transactions on Power Electronics*, 29(8):4339–4347, 2014.

[15] Mangesh Borage, Sunil Tiwari, and Swarna Kotaiah. Analysis and design of an LCL-T resonant converter as a constant-current power supply. *IEEE Transactions on Industrial Electronics*, 52(6):1547–1554, 2005.

[16] B. Reddy, G. Kumar, B. Kumar, B. Jhansi, B. Sandeep, and Sarada Kota. Fuel cell based ultra-voltage gain boost converter for electric vehicle applications. *Transactions on Energy Systems and Engineering Applications*, 4(1):68–90, 2023.